

On-sky performance of the GMT dispersed fringe phasing sensor prototype

Derek Kopon^{*a}, Brian McLeod^a, Antonin Bouchez^c, Daniel Catropa^a, Marcos A. van Dam^b, Danielle Frostig^a, Jan Kansky^a, Ken McCracken^a, William Podgorski^a, Stuart McMuldloch^a, Joseph D'Arco^a, Laird Close^d, Jared R. Males^d, Katie Morzinski^d

^aHarvard-Smithsonian Center for Astrophysics, 60 Garden Street, Cambridge, MA, 02138

^bFlat Wavefronts, 21 Lascelles St., Christchurch 8022, New Zealand

^cGMTO Corporation, 465 N. Halstead Street, Suite 250, Pasadena, CA 91107

^dSteward Observatory, University of Arizona, Tucson, AZ 85721

Abstract

The Acquisition, Guiding, and Wavefront sensing System (AGWS) serves multiple active and adaptive optics functions within the GMT. The AGWS uses four identical moveable star probes that perform target acquisition, active optics wavefront control, Shack-Hartmann ground-layer wavefront sensing, segment tip/tilt sensing, and segment phasing. With the exception of segment phasing, these tasks are performed by one of three selectable optical channels feeding an e2v CCD351 EMCCD camera. The most challenging task, segment phasing, is performed by a J-band dispersed fringe sensor (DFS). The DFS uses 1.5-meter square subapertures overlaying each of twelve ~ 40 cm segment boundary interfaces in a re-imaged pupil plane. A doublet prism array disperses the fringes formed by each segment boundary in the direction parallel to the segment gap. An optical relay images the fringes onto a SAPHIRA eAPD array that is being read out faster than the coherence time of the atmosphere. In-phase segments produce straight fringes while out-of-phase segments produce tilted fringes. This tilt is measured with the Fourier amplitude. To validate our design, we built a DFS using the same optical design, doublet prism array, and C-RED eAPD camera as our GMT design. We tested the prototype DFS on-sky at the Magellan Clay telescope during two observing runs in May and November 2018. The first run used an AO corrected beam from the MagAO system and the second used a seeing-limited beam from the F/11 facility secondary mirror. We present our on-sky results and data analysis. The tests included guide stars of varying magnitudes, AO-corrected and seeing-limited observations, and changing the zenith angle and dispersion orientation to understand the effect of differential atmospheric refraction on the measurements.

Keywords: Active optics, adaptive optics, Giant Magellan Telescope, phasing, dispersed fringe sensor, e-APD array

1. INTRODUCTION

1.1 The GMT AGWS

The 25.4-meter Giant Magellan Telescope (GMT) uses seven 8.4-meter primary segments. The AGWS¹ uses off-axis guide stars to make measurements required to keep the optics of the GMT coaligned, phased, pointing in the correct direction, and conforming to the correct mirror shape^{2,3,4} (Figure 1). The AGWS allows target acquisition with a 30 arcsec imaging mode and Shack-Hartmann wavefront sensing for ground-layer adaptive optics (GLAO)⁵. When operating in natural seeing or GLAO mode, the AGWS is the primary wavefront sensing system for the telescope. When operating in natural guide star AO mode (NGSAO), the AGWS will perform the initial phasing of the seven segment pairs. In laser tomography AO (LTAO) mode, the AGWS will keep the telescope phased over the course of the observation⁶.

The AGWS consists of four identical movable star probes located just before the telescope focal plane (Figure 2). Each star probe contains four selectable optical channels: three visible and one infrared. The three visible channels are: a 30 arcsec FOV acquisition mode; a 48x48 element Shack-Hartmann wavefront sensor capable of both active optics measurements and ground-layer wavefront sensing at 100 Hz; and a 24x24 element Shack-Hartmann channel for segment tip/tilt sensing and wavefront sensing in poor seeing and/or on faint guide stars. The IR channel is the J-band DFS that is fed by a dichroic beamsplitter.

*derek.kopon@cfa.harvard.edu

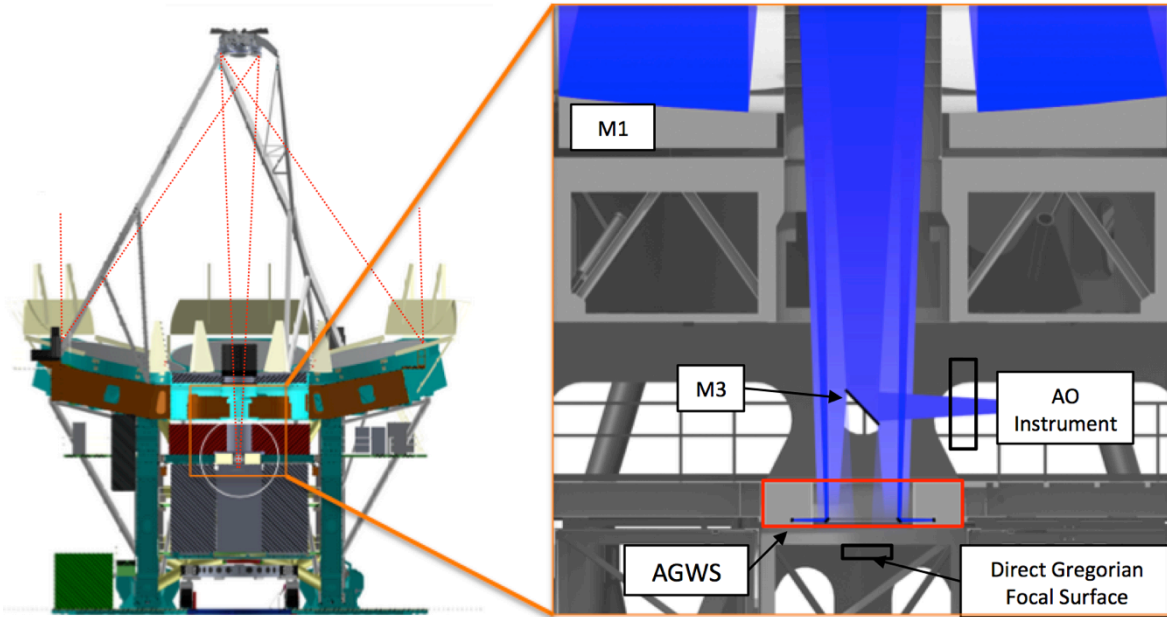


Figure 1: The AGWS location near the GMT focal plane.

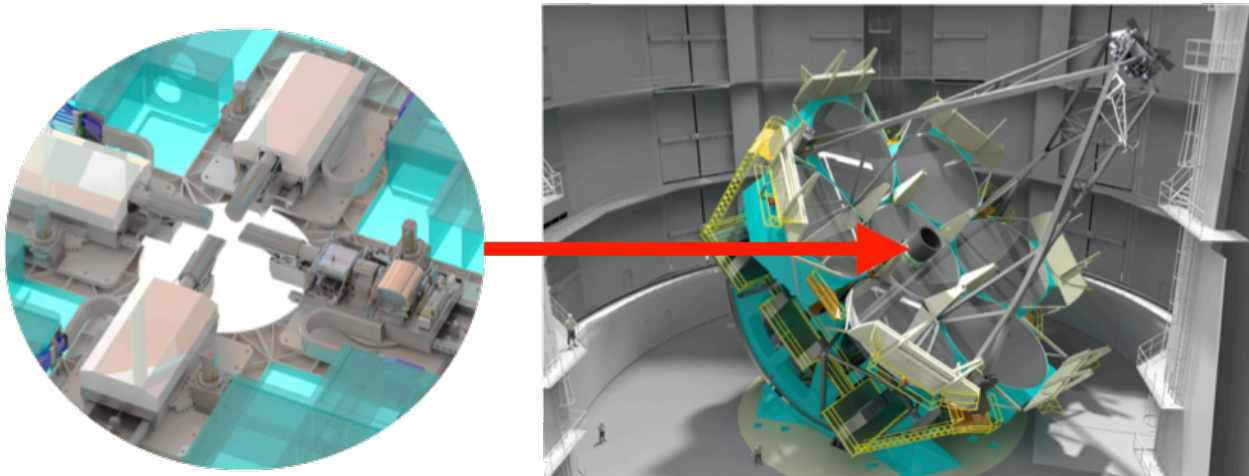


Figure 2: The four movable star probes of the AGWS mount to the GMT Gregorian Instrument Rotator.

1.2 The AGWS dispersed fringe phasing sensor

Dichroic beamsplitters in each AGWS probe will transmit visible light to be used for wavefront and tip/tilt sensing, while near-IR light is reflected to the DFS for piston phase sensing. Simulations by van Dam⁷ demonstrate the highest sky coverage will be achieved by using a J-band DFS for phasing. The DFS takes fringes produced at a segment boundary and disperses them with a doublet prism array in the direction perpendicular to diffraction. Because the locations of the minima and maxima of the fringes of the diffraction pattern vary with wavelength, the dispersed fringes are straight if the two segments are in phase. A phase shift produces a tilt in the dispersed fringes. A detector reading out faster than the coherence time of the atmospheric seeing records images of the fringes. The Fourier transform of the fringes shows a peak whose side lobe displacement is a measurement of the segment-to-segment phase difference (Figure 3). The AGWS DFS will have a total of 18 subapertures, with 12 spanning the segment boundaries, and 6 more located entirely within a segment to be used for calibration.



Figure 3: Left: The GMT pupil overlaid with 12 1.5-m square apertures at the segment boundaries. Center: Simulated fringes from one subaperture showing in phase (left) and a 10-micron phase shift (right). The dispersion direction is vertical. Right: A simulated dispersed fringe image and its FFT. The vertical displacement of the circled peak is a function of the tilt of the fringes and thus a measure of the phase error.

1.3 Previous phasing prototypes

SAO has built and tested two previous phasing prototypes on sky at Magellan. The first, in 2012, was a K-band dispersed Hartmann sensor⁸. This instrument was fed with a seeing limited F/11 beam. The fringes were tip/tilt stabilized with a fast steering mirror. The advent of the SAPHIRA sub-electron read-noise fast readout IR array allowed us to eliminate the need for tip/tilt stabilization in our current DFS design.

The second phasing prototype was a dispersed fringe sensor operating behind the Magellan AO system. The sensor was tested on sky in December 2015^{9,10}. This sensor had two wavelength channels: an I-band channel with a Princeton EMCCD camera and a J-band channel with a Ninox InGaAs detector. This prototype had a variable phase shifter located near the pupil and the ability to operate at 6 arcmin off-axis. This sensor verified that our DFS design can achieve our required 40-micron capture range of piston.

The optical design of our current prototype, known as Proto3, uses custom optics that produce well-corrected images. A phase shifter plate gives well qualified phase shifts in each of the three subaperture pairs. Lithographic phase plates give us the ability to remove the Magellan off-axis coma and simulate the GMT off-axis aberrations, primarily astigmatism. A 7-facet prototype doublet prism array allows us to disperse fringes without the stray light and spurious diffractive orders generated by the grism disperser in the previous prototype. The SAPHIRA e-APD detector (commercially available in First Light Imaging's C-RED One camera) with a custom blocking filter allows us fast sub-electron read-noise performance in the J-band.

We further retrofitted the Proto3 to accept an F/11 beam for use with the Magellan F/11 secondary. We refer to this retrofit as Proto3c.

2. THE PROTOTYPE DESIGN

2.1 Proto3 design

Our objective was to build a sensor as similar as possible to the actual sensor design that we will use at the GMT and to test it on sky under conditions that most closely mimic the conditions we expect at GMT. Our optical design is identical to the sensor we have designed for GMT, which passed PDR in 2017. The only difference in the optical design is the focal length of the collimating lens, which matches the F/16 beam of Magellan instead of the F/8 beam of GMT.

On the GMT, the AGWS will acquire guide stars in a 6-10 arcmin patrol annulus. The phasing prototype at Magellan can operate both on-axis and at 6 arcmin off-axis. At GMT, the phasing sensors will be operated while AO is being performed with the on-axis science instrument. Therefore, the off-axis sensor will see the atmospheric structure produced by an on-axis AO-corrected beam. This beam will see disproportionately higher high order turbulence due to the isoplanatic error in the off-axis beam. The Magellan AO system will correct the beam using an on-axis guide star. The MagAO system uses a thin-shell adaptive secondary and a pyramid wavefront sensor¹¹. It is one of the closest AO analogues to the GMT design that is currently operational.

At an off-axis position, the Magellan and GMT telescopes produce different static aberrations. As described later, we will statically correct the Magellan aberrations and introduce the GMT aberrations. By adjusting the Magellan instrument rotator, we will also be able to change the direction of the parallactic angle relative to the aperture mask and prism dispersion in order to measure the effects of atmospheric dispersion on the phase measurements.

2.2 Optical design

The prototype optical design is an almost identical copy of the baseline GMT design¹² (**Error! Reference source not found.**), the only difference being the focal length of the first lens element (**Error! Reference source not found.**). A collimating lens reimages the Magellan pupil onto a laser-cut mask containing pairs of segment boundary apertures (Figure 4). The aperture pairs simulate a 1.5-meter square overlaid on the segment boundaries of the Magellan pupil for three different guide star off-axis distances: 6, 8, and 10 arcmin. Because the GMT primary and secondary segments are critically sized relative to each other, an increase in off-axis distance causes vignetting that effectively increases the inter-segment spacing.

After the mask, the prototype prism doublet array follows, which disperses the beam in the direction perpendicular to the diffraction pattern formed by the segment boundary apertures. After the prism array, a three doublet optical relay images the dispersed fringes onto the detector.

The prototype will have a pupil viewing channel to allow the aperture mask to be precisely aligned to the telescope pupil and to ensure that the apertures are uniformly illuminated. There will also be an “unobscured mode” that allows the prism and mask assembly to be removed from the beam and replaced with a lens assembly in order to allow the full telescope pupil to be viewed, or an undispersed/undiffracted image to be produced. The unobscured mode will be used to calibrate the detector using an on-board flat field source. For more detail on the optical design and various operating modes of the Proto3, see Kopon et al. 2018¹³.

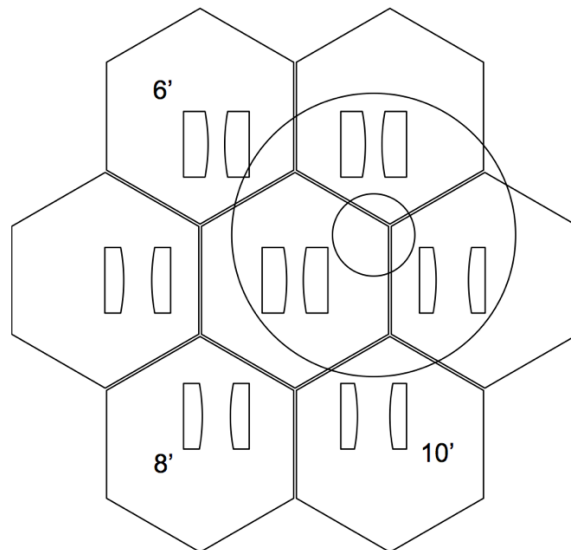


Figure 4: The pupil aperture mask overlaid with the circular Magellan pupil and the hexagonal prism array. Aperture pairs simulating GMT segment boundaries as seen by guide stars of different off-axis differences can be selected by moving the prism/mask assembly relative to the beam. Three subaperture pairs can be positioned in the telescope beam at one time.

2.3 Proto3c F/11 Retrofit

In Fall 2018, we scheduled a three-night Magellan run with the rigid facility F/11 secondary. Because the prototype was originally designed to accept an AO-corrected F/16 beam from the adaptive secondary mirror, we retrofitted the

Proto3 with additional optics in order to accept the F/11 input beam while maintaining the same working distance between the telescope focal plane and the internal pupil of the prototype.

Our design consists of an optical assembly containing one COTS singlet and two identical custom doublets. The prototype was retrofitted with this optical assembly prior to the Fall 2018 telescope and was thereafter known as Proto3c (see Figure 5).

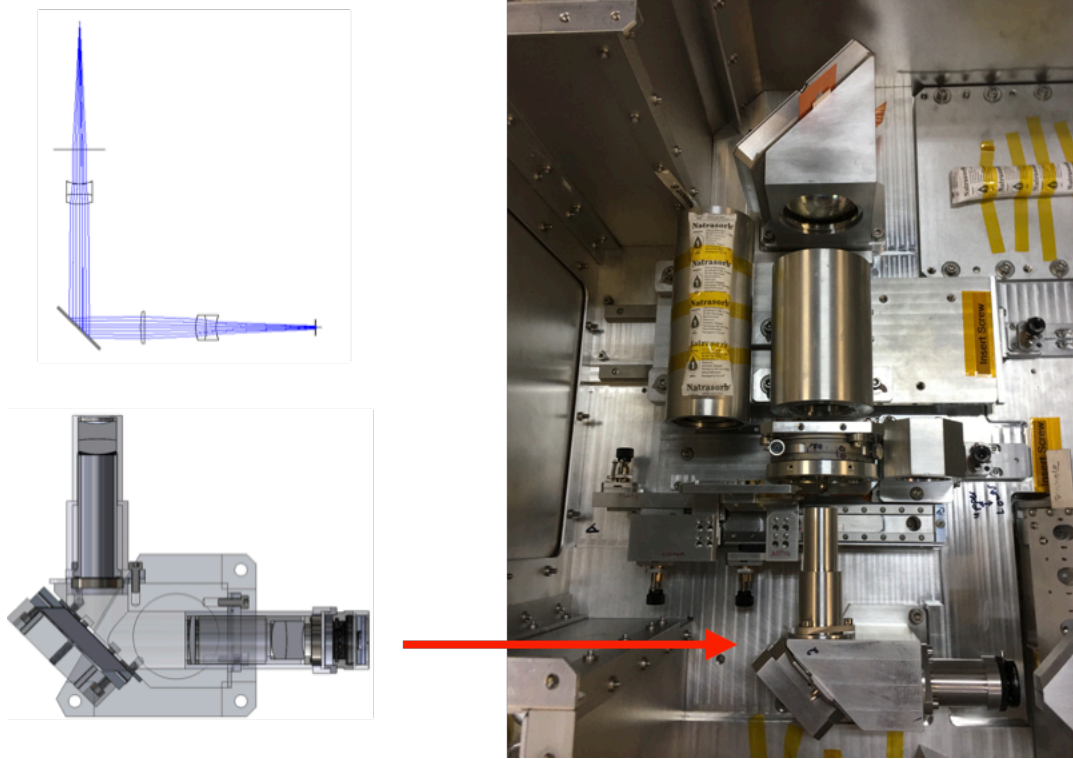


Figure 5: 3-element optical assembly installed into the phasing prototype in order to allow acceptance of F/11 beam.

2.4 Shack-Hartmann 30x30 “Truth” Sensor

In addition to the installation of the F/11 optical assembly into the phasing prototype, we also installed a new Shack-Hartmann optical tube into the facility guider probe. Our experience in the previous telescope run (spring 2018) left us uncertain if non-zero phase shifts measured by the phasing sensor were the result of miscalibration of the zero point of the phasing sensor itself, or phase shift due to wavefront errors coming from the telescope. Poor weather during the spring run prevented us from having time to take enough data to break this degeneracy. We installed a 30x30 Shack-Hartmann tube, which corresponded to a subaperture size of 0.212 meters. This is sufficiently fine pitch to sample the phase shift between our phasing subapertures in order to provide an independent verification of the phase due to telescope/atmosphere aberrations. Figure 6 shows the 30x30 Shack-Hartmann grid laid over the Magellan telescope pupil and the phasing subapertures.

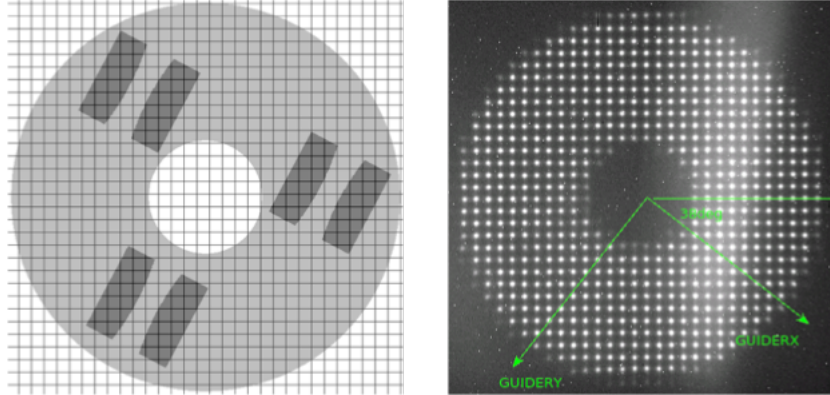


Figure 6: Left: The 30x30 Shack-Hartmann grid laid over the Magellan telescope pupil and the prototype phasing subapertures. Right: Image of the Shack spots from the telescope.

3. RESULTS

3.1 Observations

We obtained on-sky data during two three-night observing runs at the Magellan Clay telescope in 2018. The spring run used the F/16 adaptive secondary performing AO correction on a bright on-axis guide star with MagAO¹⁴. 1.5 nights of this run were lost to poor weather. The Fall run used the facility rigid F/11 secondary and a seeing-limited on-axis beam. Full data reduction of the data for these runs is presented in an internal report by van Dam et al, 2019¹⁵. Figure 7 shows sample fringe data.

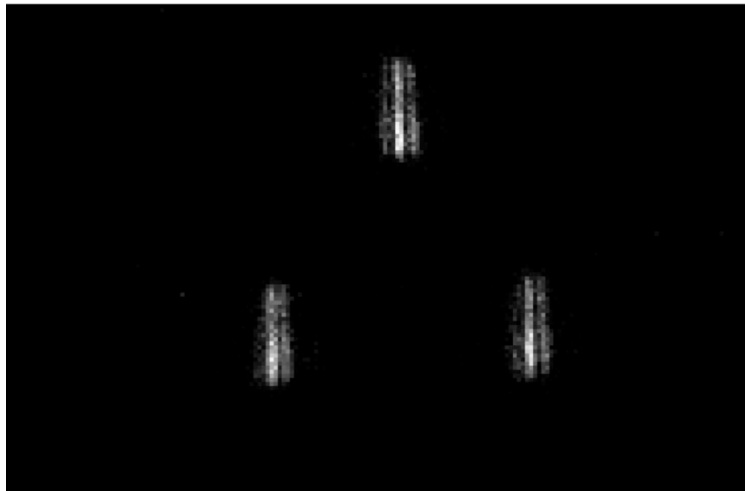


Figure 7: Sample fringe data.

3.2 Dispersed Fringe Sensor (DFS) Analysis

The DFS method of data reduction involves taking the Fourier transform of the dispersed fringes and then measuring the displacement of the side lobe in the Fourier amplitude (see Figure 8). The advantages of this technique are high sensitivity and high capture range, which work in a broad range of conditions. The disadvantage of this technique is that many effects other than piston phase errors, such as atmospheric dispersion, can cause the fringes to tilt.

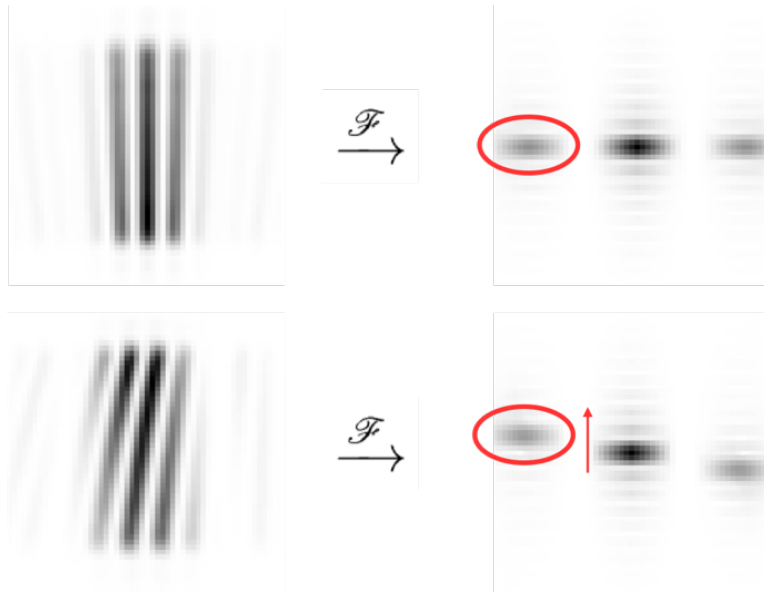


Figure 8: Left: Dispersed fringe with no phase shift (top) and with a phase shift (bottom). Right: The Fourier transform of the dispersed fringes. A phase shift causes displacement in the location of the side lobe of the Fourier Transform.

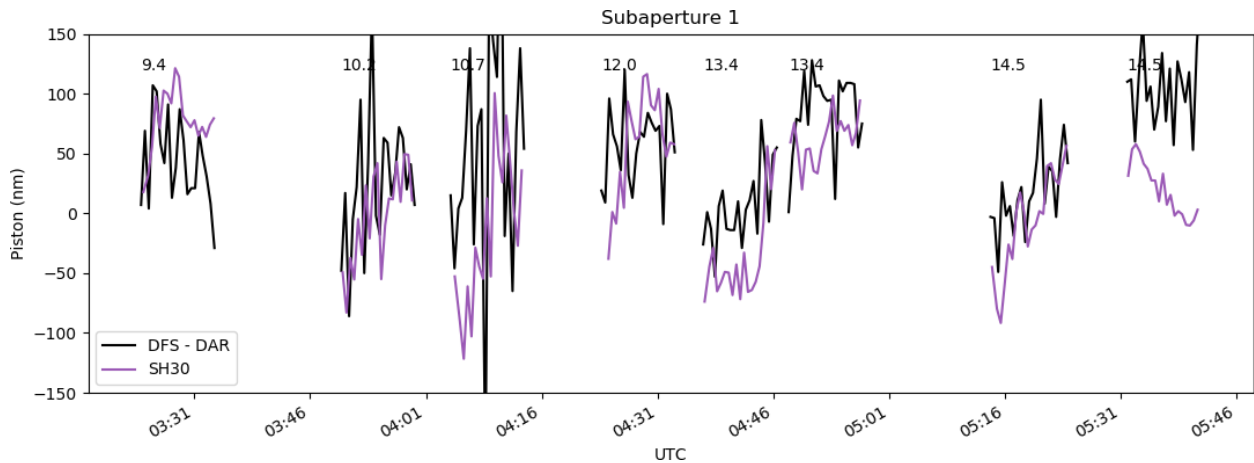


Figure 9: Data showing DFS performance as a function of guide star magnitude.

Using the DFS technique, we have demonstrated the ability to phase on faint guide stars ($m_V = 14.5$ mag in good seeing). See Figure 9.

3.3 Dispersed Hartmann Sensor (DHS) Analysis

The DHS method determines phase by looking at the Fourier phase instead of the Fourier amplitude of the fringes. This method has a much smaller capture range than the DFS method, but it does have other advantages, such as not being susceptible to atmospheric dispersion (see Figure 10).

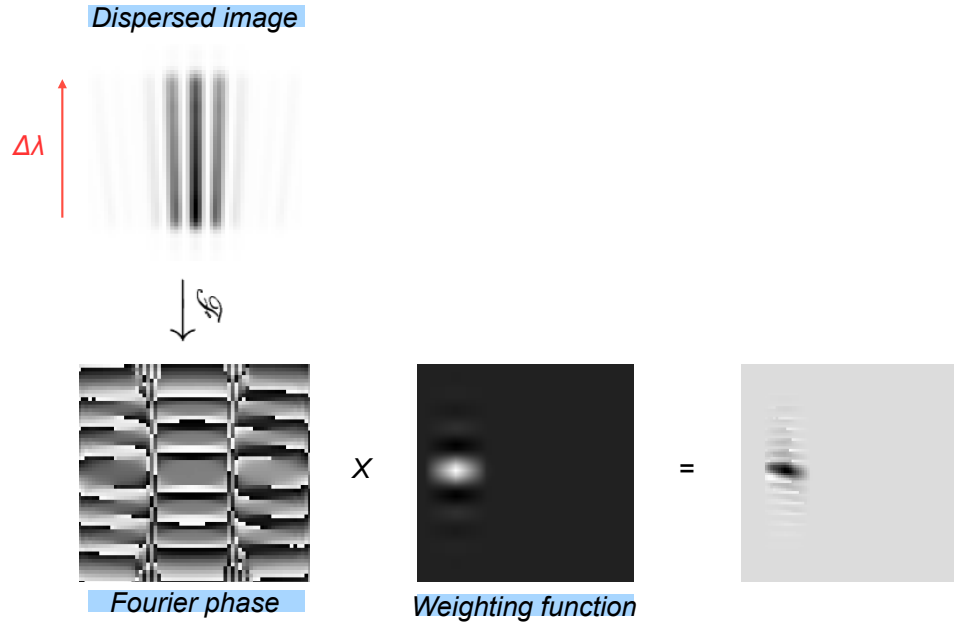


Figure 10: The DHS method uses the Fourier phase instead of the Fourier amplitude to calculate the phase shift in the dispersed fringes.

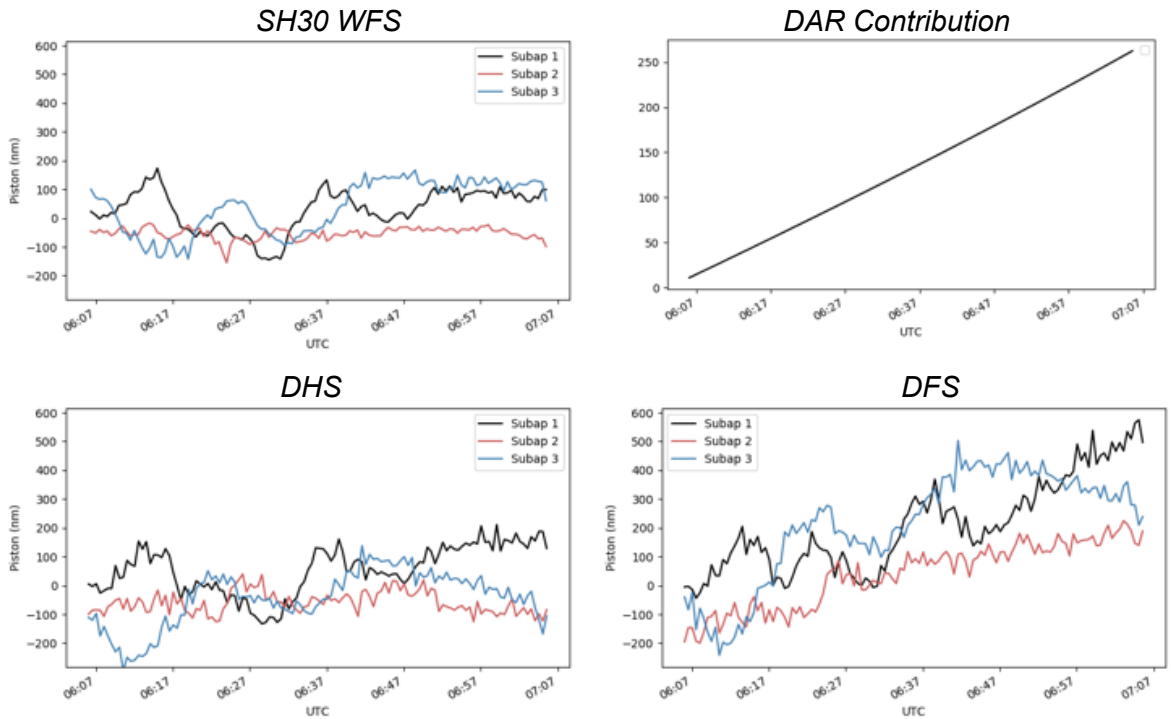


Figure 11: A representative data series from one of our nights with the F/11 seeing-limited beam. The DFS, DHS, and Shack-Hartmann methods give similar results. The DFS method is sensitive to differential atmospheric refraction, which is reflected in the data.

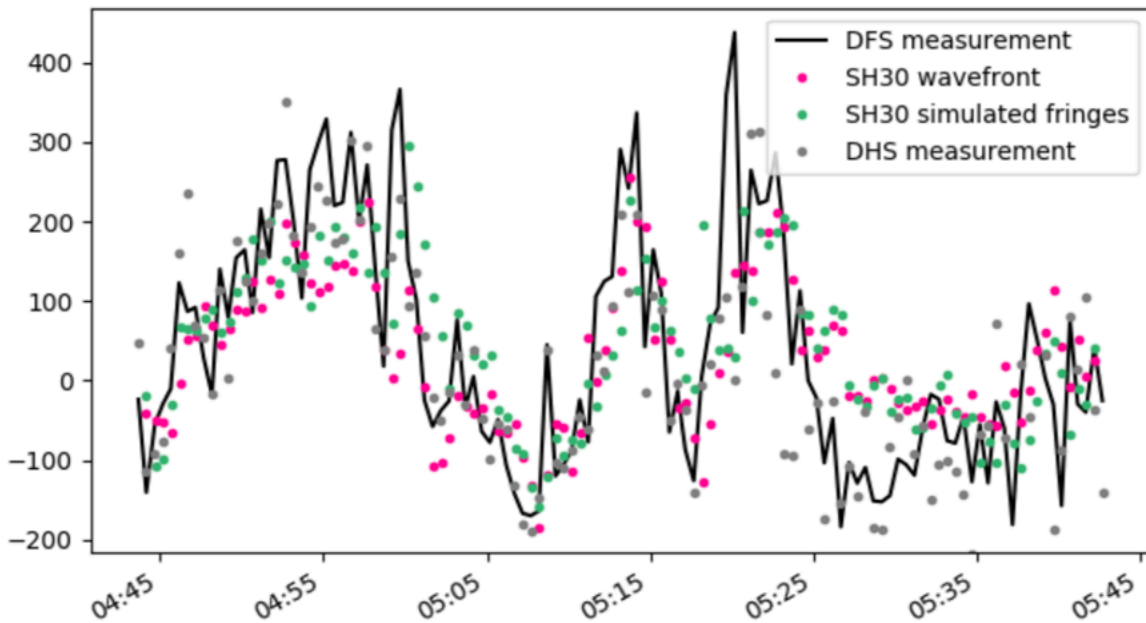


Figure 12: A representative data set showing the DFS data compared to the DHS and SH30 data. They track very well.

Figure 12 and Figure 12 show representative data series with the same data being reduced using the DFS and DHS methods. The corresponding data from the SH30 is also shown. After calibrating out differential atmospheric refraction, there is good agreement between the methods.

3.4 Knox-Thompson Analysis

The Knox-Thompson method was developed in 1974 for speckle interferometry. This is another technique that is insensitive to atmospheric dispersion. The disadvantages of this technique are a reduced capture range relative to the DFS. This technique also will not work if the subaperture gets too large, so it may not work if our probe is too far off-axis. Because the GMT secondary segments are critically sized to the primary segments, off-axis vignetting creates an effectively larger segment gap at the phasing sensor pupil. See Figure 13 and Figure 14 for representative data sets showing the agree between our various methods.

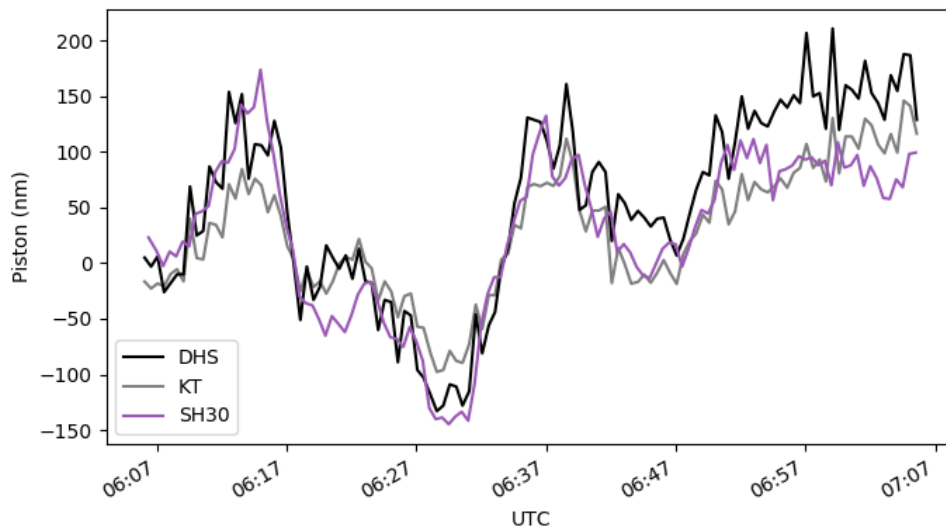


Figure 13: Representative data set comparing the Knox-Thompson method to the DHS and SH30 data.

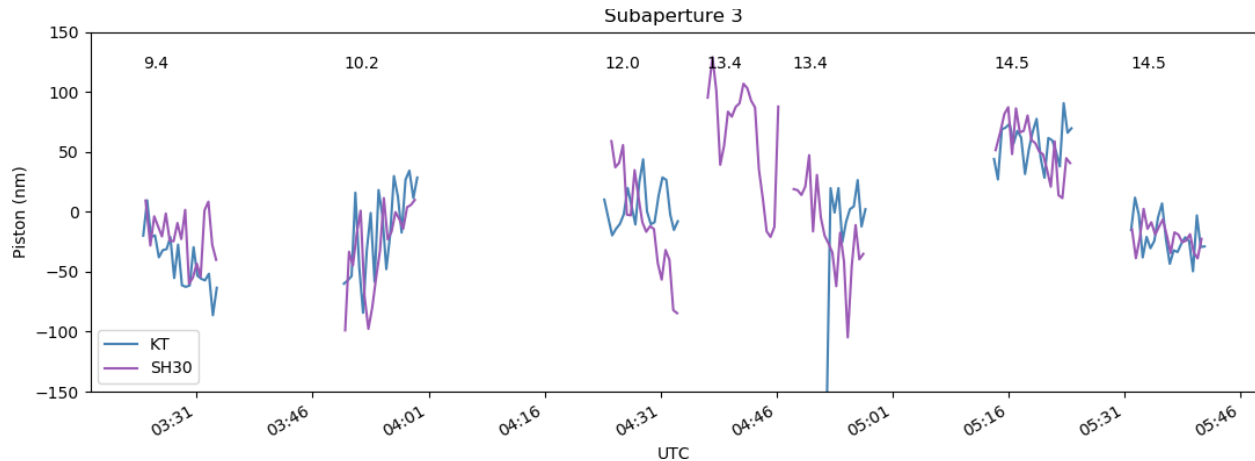


Figure 14: Data demonstrating the limiting magnitude of the Knox-Thompson method relative to the SH30 data.

4. CONCLUSIONS

Our spring 2018 run behind the MagAO adaptive system produced excellent results with the AO loop closed. However, during open-loop operation, the measured phase seemed to be dominated by quasi-static biases that we suspected were coming from the ASM. Poor weather prevented us from exploring this possibility further. In the fall 2018, we retrofitted our prototype to accept an F/11 beam from the facility rigid secondary in order to perform seeing limited on-axis observations. We also installed a fine resolution 30x30 Shack-Hartmann sensor to serve as a truth sensor. After careful calibration, we found good agreement between the dispersed fringe sensor and the SH30. We found good agreement with the DHS technique, which is insensitive to atmospheric dispersion. We also reduced the data with the Knox-Thompson method, which allows the advantage of insensitivity to differential atmospheric refraction in a host of observing conditions. We verified that our sensor has sufficient sensitivity on faint guide stars to meet our requirements. In earlier runs, we demonstrated our +/- 40 micron capture range requirement with the DFS method.

Acknowledgements

This work was supported by the GMT Corporation, a non-profit organization operated on behalf of an international consortium of universities and institutions: Arizona State University, Astronomy Australia Ltd., the Australian National University, the Carnegie Institution for Science, Harvard University, the Korea Astronomy and Space Science Institute, The Sao Paulo Research Foundation, the Smithsonian Institution, The University of Texas at Austin, Texas A&M University, University of Arizona, and University of Chicago.

REFERENCES

- [1] McLeod, B., et al., "The acquisition, guiding, and wavefront sensing system for the Giant Magellan Telescope," SPIE 10700, 10700–10760 (2018).
- [2] McLeod, B., Bouchez, A. H., Espeland, B., Filgueira, J., Johns, M., Norton, T. J., Ordway, M., Podgorski, W. A., Roll, J., et al., "The Giant Magellan Telescope active optics system," Proc. SPIE **9145**, 91451T (2014).
- [3] Quirós-Pacheco, F., Conan, R., McLeod, B., Irarrazaval, B., Bouchez, A., "Wavefront control simulations for the Giant Magellan Telescope: Field-dependent segment piston control," AO4ELT4 Conf. Proc. (2015).
- [4] Bouchez, A. H., McLeod, B. A., Acton, D. S., Kanneganti, S., Kibblewhite, E. J., Shtetman, S. A., van Dam, M. A., "The Giant Magellan Telescope phasing system," Proc. SPIE **8447**, 84473S (2012).
- [5] Bouchez, A., et al., "An overview and status of the GMT adaptive and active optics," Proc. SPIE 10703, 10703–10733 (2018).
- [6] Quirós-Pacheco, F., et al., "The Giant Magellan telescope phasing strategy and performance," Proc. SPIE 10700, 10700–10718 (2018).
- [7] van Dam, M. A., McLeod, B. A., Bouchez, A. H., "Dispersed fringe sensor for the Giant Magellan

- Telescope," *Appl. Opt.* **55**(3), 539–547, OSA (2016).
- [8] Kanneganti, S., McLeod, B. A., Ordway, M. P., Roll, J. B., Shtetman, S. A., Bouchez, A. H., Codona, J., Eng, R., Gauron, T. M., et al., "A prototype phasing camera for the Giant Magellan Telescope," *Proc. SPIE* **8447**, 844710–844752 (2012).
- [9] Kopon, D., McLeod, B., van Dam, M. A., Bouchez, A., McCracken, K., Catropa, D., Podgorski, W., McMuldroy, S., Conder, A., et al., "On-sky demonstration of the GMT dispersed fringe phasing sensor prototype on the Magellan Telescope," *Proc. SPIE* **9909**, 990911–990946 (2016).
- [10] Kopon, D., McLeod, B., McCracken, K., van Dam, M., Bouchez, A., Conder, A., Podgorski, W. A., Catropa, D., McMuldroy, S., et al., "Prototyping the GMT phasing camera with the Magellan AO system," *AO4ELT4* (2015).
- [11] Close, L. M., Males, J. R., Morzinski, K., Kopon, D., Follette, K., Rodigas, T. J., Hinz, P., Wu, Y.-L., Puglisi, A., et al., "Diffraction-limited Visible Light Images of Orion Trapezium Cluster with the Magellan Adaptive Secondary Adaptive Optics System (MagAO)," *ApJ* **774**, 94 (2013).
- [12] Kopon, D., et al., "Phasing the GMT with a next generation e-APD dispersed fringe sensor: design and on-sky prototyping," *AO4ELT5* (2017).
- [13] Kopon, D., McLeod, B., Bouchez, A., Catropa, D., Dam, M. A. van., Frostig, D., Kinsky, J., McCracken, K., Podgorski, W., et al., "Preliminary on-sky results of the next generation GMT phasing sensor prototype," *Proc. SPIE* **10703**, 107030X-10703–10714 (2018).
- [14] van Dam, M., McLeod, B., Kinsky, J., Bouchez, A., "FWN 102: Analysis of Proto3 on-sky data" (2018).
- [15] van Dam, M., McLeod, B. A., Kinsky, J., Kopon, D., Bouchez, A., "FWN 106: Analysis of Proto3c On-Sky Data," internal design report (2019).